Journal of Magnetic Resonance 193 (2008) 218–225

Contents lists available at ScienceDirect

Journal of Magnetic Resonance

journal homepage: www.elsevier.com/locate/jmr

Determining NMR flow propagator moments in porous rocks without the influence of relaxation

J. Mitchell [a], D.A. Graf von der Schulenburg [a], D.J. Holland [a], E.J. Fordham [b], M.L. Johns [a], L.F. Gladden [a,*]

[a] Department of Chemical Engineering, University of Cambridge, Pembroke Street, Cambridge CB2 3RA, UK
[b] Schlumberger Cambridge Research, High Cross, Madingley Road, Cambridge CB3 0HG, UK

ARTICLE INFO

Article history:
Received 12 March 2008
Revised 29 April 2008
Available online 6 May 2008

Pacs:
05.60.-k
07.05.Hd
76.60.-k
76.60.Es
76.60.Jx
76.60.Lz
76.60.Pc
47.11.+j
47.55.Mh
47.80.+v

Keywords:
Flow
Propagators
Relaxation
Displacement-T2 correlation
T1-displacement correlation
Laplace–Fourier transform
Permeable rocks

ABSTRACT

Flow propagators, used for the study of advective motion of brine solution in porous carbonate and sandstone rocks, have been obtained without the influence of Nuclear Magnetic Resonance (NMR) relaxation times, T_1 and T_2. These spin relaxation mechanisms normally result in a loss of signal that varies depending on the displacement ζ of the flowing spins, thereby preventing the acquisition of quantitative propagator data. The full relaxation behaviour of the system under flow needs to be characterised to enable the implementation of a true quantitative measurement. Two-dimensional NMR correlations of $\zeta - T_2$ and $T_1 - T_2$ are used in combination to provide the flow propagators without relaxation weighting. $T_1 - \zeta$ correlations cannot be used due to the loss of T_1 information during the displacement observation time Δ. Here the moments of the propagators are extracted by statistical analysis of the full propagator shape. The measured displacements (first moments) are seen to correlate with the expected mean displacements for long observation times Δ. The higher order moments of the propagators determined by this method indicate those obtained previously using a correction were overestimated.

1. Introduction

Nuclear Magnetic Resonance (NMR) flow propagator measurements [1] yield useful information on the hydrodynamic dispersion of fluids flowing through porous media [2]. For this reason they have been used in the study of oil-bearing rocks [2–5] for the purpose of improving the understanding of oil recovery processes. By observing the displacement ζ of encoded spins over a range of observation times Δ and superficial flow velocities Q, the fluid behaviour and pore-scale heterogeneity can be characterised through the analysis of the propagator moments [2]. However, these results are affected by the relaxation time constants of the spins being observed. In order to effectively remove the relaxation time weighting from the propagators the longitudinal (T_1) and transverse (T_2) relaxation times need to be fully characterised for the entire spin population under the relevant conditions of flow. T_2 relaxation can be determined as a function of displacement in a two-dimensional $\zeta - T_2$ correlation experiment. This technique has been previously used in the study of fluid flowing in pipes and bead packs [6,7]. $\zeta - T_2$ correlations have also been used by Windt et al. [8] to remove transverse relaxation weighting in spatially resolved studies of flow in biological systems, where the displacement was encoded using the simpler pulsed gradient spin echo (PGSE) [9] sequence. However, the equivalent correlation for T_1 and displacement, $T_1 - \zeta$, cannot be used to determine the T_1 behaviour. At long Δ, when Δ is greater than the average relaxation time $\langle T_1 \rangle$ of the sample, the longitudinal relaxation information is lost due to magnetisation decay during the observation time of the stimulated echo [10] which is an inherent part of the

* Corresponding author.
E-mail address: lfg1@cam.ac.uk (L.F. Gladden).

1090-7807/$ - see front matter © 2008 Elsevier Inc. All rights reserved.
doi:10.1016/j.jmr.2008.05.001

required Alternating Pulsed Gradient Stimulated Echo (APGSTE) sequence [11]. At short Δ, where $\Delta \leqslant \langle T_1 \rangle$, the long recovery delays in the T_1 encoding portion of the sequence will be sensitive to motions averaged over large displacements regardless of the short observation time. This problem persists even if the order of encoding is reversed in a $\zeta - T_1$ correlation because the observation time of the stimulated echo still acts as an additional T_1 recovery delay. Potentially, this situation could be overcome by utilising the PGSE sequence to encode displacement. However, the stimulated echo is required in the experiments described here to observe the long-time behaviour (on the order of seconds) of the flowing system. The spin echo observation time is limited by T_2 relaxation, whereas the stimulated echo observation time is limited by T_1; $T_1 \gg T_2$ typically in water saturated rock cores.

Instead of acquiring $T_1 - \zeta$ correlations, a correlation between T_1 and T_2 can be determined under the conditions of flow. Assuming a unique T_1 relaxation time component can be determined for each T_2 relaxation time component, the $\zeta - T_2$ correlation can be used subsequently to remove all the relaxation time weighting in the propagators. The correct propagator probability distribution (without relaxation weighting) will be denoted here as $P^*(\zeta^*, \Delta)$.

NMR propagators consist of a probability distribution $P(\zeta, \Delta)$ describing the displacement ζ of spins moving with a mean pore velocity v_p, during an observation time Δ. The NMR signal obtained from the conventional APGSTE sequence [11] will also contain a weighting according to the T_1 and T_2 relaxation times. These probability distributions are distorted unevenly because the signal lost from relaxing spins will vary as a function of displacement. There are two key mechanisms by which the spins, associated with a liquid phase, will relax more rapidly in a porous medium. Slow moving spins in stagnant, geometrically smaller regions are more likely to collide with the pore wall and couple to relaxation sinks, such as paramagnetic species in the rock. Fast moving spins may be associated with an enhanced relaxation process due to their displacement through magnetic field gradients resulting from magnetic susceptibility differences in the pore space, or magnet (B_0) inhomogeneities. The relaxation of the stagnant spins is usually the dominant relaxation mechanism. The result of this is an apparent increase in the observed mean displacement $\langle \zeta \rangle$ relative to the expected mean displacement $\langle \zeta \rangle_0$. This is denoted by the parameter $\theta = \langle \zeta \rangle / \langle \zeta \rangle_0$, such that $\theta > 1$ at long observation times [2]. Scheven et al. proposed a simple "delta-function" correction, centred on $\zeta = 0$, to the probability distribution [2]. This was based on the assumptions that spins lost to surface relaxation were stagnant over all values of Δ, and that all flowing spins had an equal probability of relaxation due to magnetic field fluctuations. This provided a corrected probability distribution of $P'(\zeta') = (1 - \theta^{-1})\,\delta_{dd}(\zeta) + \theta^{-1} P(\zeta)$, where $\delta_{dd}(\zeta)$ is a Dirac delta function. This "delta-function" correction describes an extreme case where the spectral weight of the distribution is altered only at $\langle \zeta \rangle = 0$. The actual relaxation behaviour of the spins will cause the spectral weight to vary as a function of displacement.

The dispersivity of a fluid flowing through porous media can be determined by analysing the second and third central moments of the probability distributions. These are equivalent approximately to the normalised root-mean-square (rms) width $\sigma / \langle \zeta \rangle$ and normalised skewness defined as $\gamma / \langle \zeta \rangle$ [2]. In the limit of pure diffusive motion the probability distribution will be Gaussian in shape. At the opposite asymptotic extreme, under the condition of full mechanical dispersion where the spin population is advected a mean distance $\langle \zeta \rangle$, the probability distribution is also characterised by a Gaussian such that $\sigma^2 = 2 D_M \langle \zeta \rangle$ where D_M is the dispersivity. In general, the normalised rms width will be characterised by $\sigma / \langle \zeta \rangle = (\langle \zeta \rangle / l)^{\eta}$. For a Newtonian fluid, this power-law relation describes the pore-scale heterogeneity present in the rock [2] and hence provides a quantitative characterisation of the pore structure over varying length scales. The exponent η is related to the degree of mechanical mixing; in the pre-asymptotic regime $-0.5 < \eta < 0$ [12]. A displacement l occurs when $\sigma = \langle \zeta \rangle$ and this length scale provides an indication of the dispersivity D_M of the flow.

The first three moments of flow propagator probability distributions have been determined previously via a self-consistent cumulant analysis [2,13]. The mean and skewness are obtained from the phase angle of the data ϕ, and the rms width is obtained from the absolute signal amplitude — $S(q)$ — where q is the magnitude of the magnetisation wave vector. This analysis allows the moments to be extracted from a narrow range of q-space [14] defined by the nth moment of q^n up to $n = 3$. This optimised data acquisition has been demonstrated to work in conjunction with the rapid DiffTrain pulse sequence [15] to provide the moments in time sensitive measurements of flow through porous rocks [16]. In this work we extract the mean, rms width, and redefined skewness from a basic statistical analysis of the propagator probability distributions once the relaxation time weightings have been removed. It is necessary to assume T_1 is not a function of observation time Δ in order to extract the probability distributions from the $\zeta - T_2$ and $T_1 - T_2$ distributions. Notwithstanding, we demonstrate the feasibility of obtaining accurate moments up to the third order without relaxation weighting and compare these to the equivalent moments extracted from uncorrected APGSTE measurements, and moments determined via the "delta-function" correction.

2. Methodology

2.1. Materials

The rocks used in this study were Portland carbonate and Bentheimer sandstone. These are both high permeability rocks with porosities of $\varphi = 0.19$ and $\varphi = 0.22$, respectively. The carbonate is a highly heterogeneous material whereas the pore structure of the sandstone is more regular [2]. Both rock types exhibit comparatively low internal magnetic field susceptibility gradients [17]. A 3 wt% KCl brine solution was pumped through the rocks to prevent osmotic swelling of the clay content in the sandstone. The rock cores were cylindrical with a mean diameter of 38 mm and a length of 70 mm. The cores were prepared for analysis first by drying, and then they were encapsulated in Perspex under vacuum, to prevent fluid transport across the surface of the cores, before being saturated with brine. Distributor plates were added at each end of the Perspex cells to provide even flow across the entire sample cross-section.

The brine was pumped continuously through the rock cores using a dual-cylinder piston pump [Teledyne ISCO Inc., USA; model D-250] with imposed superficial volumetric flow velocities of $Q = 1, 2, 5, 9$, and 16 ml min^{-1}. The expected mean displacement $\langle \zeta \rangle_0 = v_p \Delta$ can be calculated for a given mean pore velocity and observation time. The mean pore velocity is determined from

$$v_p = \frac{Q}{A\varphi}, \tag{1}$$

where A is the sample cross-sectional area. In these experiments the direction of flow is along the z-axis of the static magnetic field. Maximum mean pore velocities of $v_p = 1306.4$ μm s^{-1} and 1068.9 μm s^{-1} were obtained in the carbonate and sandstone rocks, respectively. These velocities were limited by the pressure drop across the rock samples.

2.2. NMR experiments

The APGSTE pulse sequence [11] can be seen in Fig. 1(a). Examples of appropriate phase cycles can be found in Ref. [18,19]. This

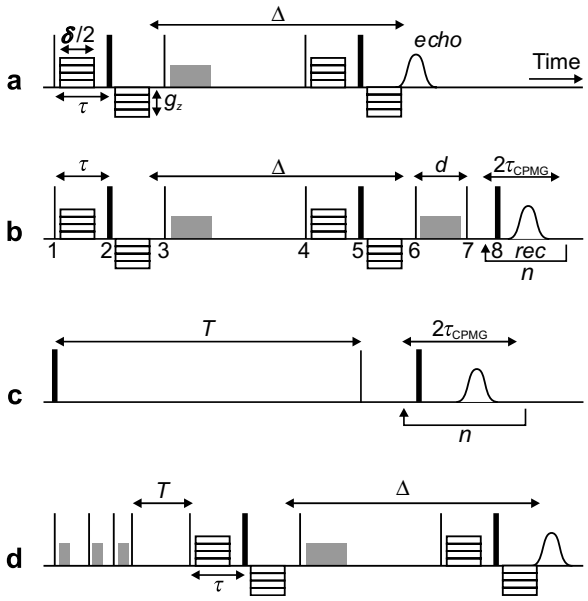

Fig. 1. Pulse sequences for (a) the APGSTE propagator measurement; (b) the $\zeta - T_2$ correlation; (c) the $T_1 - T_2$ correlation; and (d) the $T_1 - \zeta$ correlation. An appropriate phase cycle for (b) is given in Table 1 corresponding to the indices under each pulse. In all cases the solid vertical lines correspond to 90° (thin) and 180° (thick) pulses. Stepped gradients are indicated by banded rectangles. Solid grey rectangles indicate homospoil gradients. The NMR signal is acquired at the centre of each echo.

sequence was used to determine the uncorrected flow propagator probability distributions $P(\zeta,\Delta)$. The sequence consists of two pairs of bipolar gradient pulses, each pulse being of duration $\delta/2$ and strength g_z, to encode and decode the spins before and after the observation time Δ, respectively. The application of the split gradient reduces the influence of susceptibility induced magnetic field distortions [11]. The spin ensemble is stored along the z-axis for a time Δ during which the spins undergo T_1 relaxation. The pulse sequence is repeated as the gradient strength is incremented between $\pm g_z^{max}$ to probe the maximum range of q-space available. The probability distribution is obtained from the NMR signal $S(q) = \int \mathrm{P}(\zeta,\Delta)\exp(2\pi i q\zeta)\mathrm{d}\zeta$ by an inverse Fourier transform (FT). In this pulse sequence T_2 relaxation occurs over the time 4τ and T_1 relaxation occurs over the time Δ.

To provide the distribution of T_2 relaxation times as a function of displacement ζ the APGSTE pulse sequence was modified with the addition of a Carr–Purcell Meiboom–Gill (CPMG) [20] echo train consisting of n echoes, see Fig. 1(b) [6]. In order to provide a constant echo spacing of $2\tau_{CPMG}$, an additional stimulated echo (z-store) of duration d was incorporated [19]. Without this additional storage interval the first echo will occur after a time 2τ whilst the second and all subsequent echoes occur after a time $2\tau_{CPMG}$. By necessity, $\tau \gg \tau_{CPMG}$ in these measurements. However, this is merely a "cosmetic" feature to ensure the echo spacing in the CPMG data is uniform. The data could be acquired without the second stimulated echo. A single complex data point was acquired from the centre of every even echo to reduce the effect of imperfect 180° pulses. The 8-step phase cycle shown in Table 1 was employed. This was modified from one presented by Amin et al. [18] by switching the phase of the second z-store pulse (number 6 in Fig. 1) from $-x$ to $-y$ during the second half of the phase cycle. This ensures the phase information essential to the displacement measurement, encoded during the first stimulated echo, is retained across the second storage interval d.

The $T_1 - T_2$ relaxation correlation pulse sequence, shown in Fig. 1(c) consists of an inversion (180°) pulse followed by a delay T and then a CPMG echo train containing n pulses separated by an inter-echo spacing of $2\tau_{CPMG}$. A single complex data point was again acquired from the centre of every even echo.

Table 1
Phase cycle used in the $\zeta - T_2$ correlation pulse sequence shown in Fig. 1(b)

Pulse	Phase							
1	x	x	y	y	$-x$	$-x$	$-y$	$-y$
2	y	$-x$	$-x$	$-y$	$-y$	x	x	y
3	x							
4	$-x$	$-x$	$-y$	$-y$				
5	$-y$	$-y$	x	x				
6	$-x$	$-x$	$-x$	$-x$	$-y$	$-y$	$-y$	$-y$
7	x	x	x	x	y	y	y	y
8	y	y	$-y$	$-y$	$-x$	$-x$	x	x
rec	x	$-x$	x	$-x$	$-x$	x	$-x$	x

The pulse indices (1–8) refer to the numerical assignments under each of the pulses in Fig. 1(b) and the corresponding receiver phase is given by *rec*. This is an 8-step phase cycle. Any phase lists with less than 8 steps are repeated, verbatim, as required to complete the cycle.

Although not used to remove the relaxation weighting in the propagators, the $T_1 - \zeta$ correlation pulse sequence is also shown in Fig. 1(d) for completeness. This sequence consists simply of a series of 90° saturation pulses followed by a variable recovery delay T added to the beginning of the APGSTE sequence. Since the APGSTE portion of the experiment occurs after the T_1 encoding portion it is independent of the phase of the saturation pulses and so a typical 13-interval phase cycle can be used. In practice, T_1 relaxation occurs over a time $T + \Delta$, where the magnetisation recovers during time T and decays during time Δ, so if Δ is long compared to T the T_1 information will be lost before the signal is acquired. Consequently the $T_1 - \zeta$ correlation cannot be used to determine T_1 as a function of ζ for long Δ.

All measurements were conducted on an 85 MHz (^{1}H) horizontal imaging magnet controlled by a Bruker AV spectrometer. Any variables with the same name in Fig. 1 had the same value in each of the pulse sequences shown. The maximum available gradient strength was $g_z^{max} = 10.7$ G cm^{-1}. The gradients were ramped between $\pm g_z^{max}$ in 128 equal steps. All the gradient pulses were of duration $\delta/2 = 2$ ms. The inter-pulse encoding time was set at $\tau = 4$ ms (the minimum possible time to incorporate the gradient pulses) to minimise signal loss due to T_2 dephasing. The observation time Δ ranged from 100 ms to 4 s. Where CPMG echo trains were used, the inter-echo spacing $2\tau_{CPMG} = 2$ ms and $n = 1024$ echoes, providing an acquisition time spanning 4 ms to 2 s. In Fig. 1(b) the additional storage interval $d = 3$ ms: sufficient to apply the homospoil gradient pulse whilst ensuring $d \leqslant \tau$. Where a T_1 relaxation interval was employed, T varied logarithmically between $T = 10$ ms and 10 s in 32 steps.

3. Data analysis

To accurately determine the NMR signal without the influence of relaxation, the signal has to be rescaled, equivalent to the echo in Fig. 1(a) being acquired at zero time. In the APGSTE experiment, as defined in Section 2.2, T_2 relaxation occurs over a time $4\tau = 16$ ms prior to the acquisition of the signal. To analyse the T_2 relaxation as a function of displacement, the time axis in the $\zeta - T_2$ data was shifted by 16 ms accordingly. The T_2 relaxation behaviour was obtained by applying a one-dimensional Laplace inversion to each of the CPMG decay curves, following an FT of the displacement axis [6]. Negative T_2 modes observed previously in $\zeta - T_2$ correlations for flow in a pipe [6] and in bead packs [6,7] were not observed in any of these rock studies and the CPMG decays were well fitted by positive components in all cases. To determine the probability function without T_2 relaxation, it is then a simple matter of integrating along the T_2 axis of the two-dimensional correlation plot.

To remove the T_1 relaxation from the $\zeta - T_2$ distribution, $T_1 - T_2$ correlations were used to determine the mean variation of T_1 as a function of T_2, $\langle T_1/T_2 \rangle$, at each of the superficial flow velocities. These two-dimensional data sets were inverted using a fast Laplace inversion algorithm [22]. From the $\langle T_1/T_2 \rangle$ values the correct signal intensity could be restored in the $\zeta - T_2$ plots by scaling the data according to the recovery interval ($\Delta + d$) and the T_1 relaxation time for each value of T_2. The subsequent integral along the T_2 axis of the two-dimensional correlation plot provided the probability distribution $P^*(\zeta^*, \Delta)$ without any relaxation weighting; the star (*) symbol denotes a function or variable which has no relaxation weighting.

The moments of the probability distributions without relaxation weighting were obtained via a basic statistical analysis of the propagator shapes in such a way as to be consistent with the moments obtained via the cumulant analysis. The mean displacement $\langle \zeta^* \rangle$ was simply the mean value of the distribution. The rms width and skewness, as defined in Ref. [2], were determined by

$$\sigma^{*2} = \frac{\sum_i P_i^* \left(\zeta_i^* - \langle \zeta_i^* \rangle\right)^2}{2\sum_i P_i^*}, \tag{2}$$

and

$$\gamma^{*3} = \frac{\sum_i P_i^* \left(\zeta_i^* - \langle \zeta_i^* \rangle\right)^3}{6\sum_i P_i^*}, \tag{3}$$

respectively. When using the cumulant analysis, the "delta-function" corrected rms width and skewness, denoted by a prime ($'$) symbol, were derived from the uncorrected moments (measured using the APGSTE sequence) by

$$\sigma'^2 = \frac{\sigma^2}{\theta} + \langle \zeta \rangle^2 \frac{\theta - 1}{\theta}, \tag{4}$$

and

$$\gamma'^3 = \frac{\gamma^3}{\theta} + 3\langle \zeta \rangle \sigma^2 \frac{\theta - 1}{\theta^2} + \langle \zeta \rangle^3 \frac{(\theta - 1)(\theta - 2)}{\theta^3}, \tag{5}$$

respectively [2].

4. Results and discussion

4.1. Flow propagators

A selection of the $\zeta - T_2$ correlations obtained at an observation time $\Delta = 1$ s are shown in Fig. 2 for the (a–c) carbonate and (d–f) sandstone with the superficial flow velocities of (a,d) $Q = 1$ ml min^{-1}, (b,e) 5 ml min^{-1}, and (c,f) 16 ml min^{-1}. The displacement (vertical) axes have all been normlised to $\langle \zeta \rangle / \langle \zeta \rangle_0$. To the right of each plot is the projection onto the ζ axis, revealing the propagator probability distribution without T_2 weighting; the intensities are scaled to the dimensionless quantity $P \times \langle \zeta \rangle_0$, where P is the probability of a spin moving a distance ζ. Considering first the carbonate rock, Fig. 2(a–c), the mean T_2 of the flowing fraction of the spin population (where $\langle \zeta \rangle / \langle \zeta \rangle_0 \geqslant 0.5$) decreases from $\langle T_2 \rangle = 0.28$ s at $Q = 1$ ml min^{-1}, to $\langle T_2 \rangle = 0.15$ s at $Q = 16$ ml min^{-1}. This is likely attributable to the faster flowing spins passing through susceptibility induced magnetic field fluctuations and hence undergoing enhanced relaxation. In future work we will explore the transverse relaxation of the fast flowing spins at low-fields where the susceptibility gradients are less significant. The width of the T_2 distribution describing the stagnant spin population (around $\langle \zeta \rangle / \langle \zeta \rangle_0 = 0$) tends to broaden with increasing flow rate, rather than shift to lower values of T_2. From the projected probability distributions it can be seen that a significant stagnant peak remains even at the highest superficial flow velocity. Now considering the sandstone rock, Fig. 2(d–f), a similar reduction in the mean T_2 of the flowing fraction of the spin population is observed with increasing flow rate, such that $\langle T_2 \rangle = 0.3$ s at $Q = 1$ ml min^{-1}, to $\langle T_2 \rangle = 0.18$ s at $Q = 16$ ml min^{-1}. The width of the T_2 distribution does not change significantly with displacement, and the stagnant portion of the spin population has a T_2 distribution only slightly wider than that of the flowing portion. From the projected probability distributions the dominant portion of the signal can be seen to arise from the flowing spins rather than the stagnant spins at the highest superficial velocity, indicative of the more homogeneous pore structure in the sandstone compared to the carbonate.

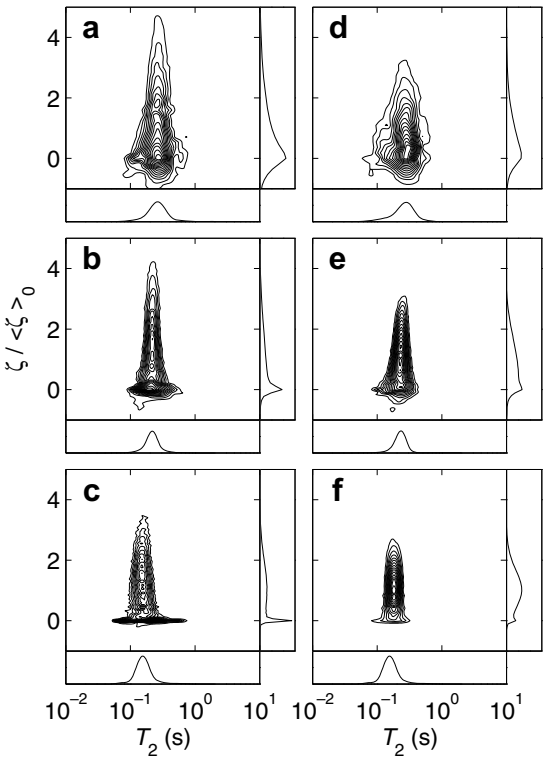

Fig. 2. Displacement–relaxation correlations, $\zeta - T_2$ for brine flowing through (a–c) carbonate and (d–f) sandstone rock cores with imposed flow velocities of (a and d) $Q = 1$, (b and e) 5, and (c and f) 16 ml min^{-1}, for an observation time of $\Delta = 1$ s. The contour intervals are the same in all the plots. The projections onto the ζ axis of each plot are shown to the right for clarity and have an intensity described by the dimensionless function $P \times \langle \zeta \rangle_0$. The projections onto the T_2 axis of each plot are also shown and have an intensity described by the dimensionless function $P\log(T_2/\mathrm{s})$.

The corresponding $T_1 - T_2$ correlations obtained are shown in Fig. 3 for the (a–c) carbonate and (d–f) sandstone with the superficial flow velocities of (a,d) $Q = 1$ ml min^{-1}, (b,e) 5 ml min^{-1}, and (c,f) 16 ml min^{-1}. In all six plots two peaks can been seen lying below the diagonal line $T_1 = T_2$. The ranges of T_2 times covered by the dominant peaks matches the ranges of T_2 times observed in the corresponding $\zeta - T_2$ plots in Fig. 2, as seen by the density of the contour levels. In all cases the dominant peaks in Fig. 3 at long T_1 and T_2 times contain over 96% of the total signal intensity. The minor peaks seen at short T_1 and T_2 times contain less than 3–4% of the total signal intensity and exhibit virtually the same relaxation times for all superficial velocities of $Q > 1$ ml min^{-1}. There is no corresponding minor peak with equivalent relaxation times in the $\zeta - T_2$ correlation plots, Fig. 2; this is not surprising since the combination of T_1 and T_2 relaxation during the APGSTE encoding portion of the pulse sequence, Fig. 1(b), would remove this fraction of the spin ensemble from the acquired signal. It is possible that the two peaks correspond to two regions of porosity: the peaks

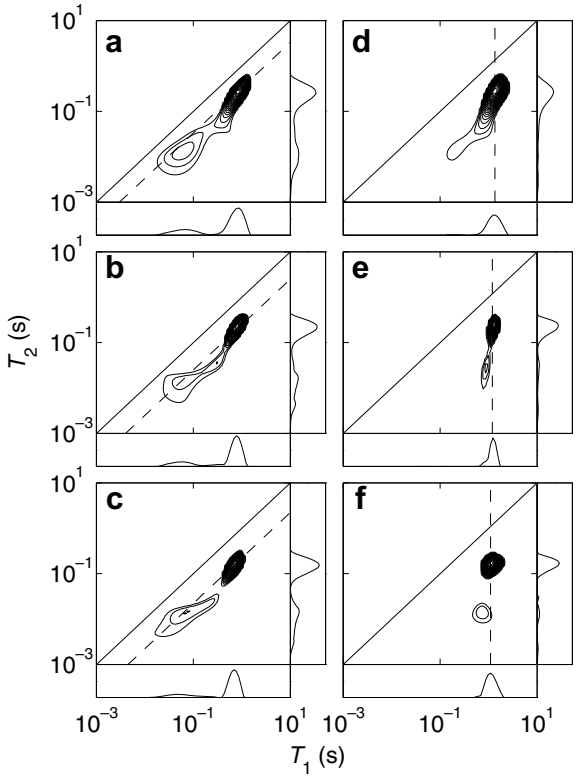

Fig. 3. $T_1 - T_2$ relaxation correlation plots for brine flowing through (a–c) carbonate and (d–f) sandstone rock cores with imposed flow velocities of (a and d) $Q = 1$, (b and e) 5, and (c and f) 16 ml min^{-1}. The central diagonal lines indicate where $T_1 = T_2$. In the carbonate plots (a–c) the lower dashed diagonal lines represent the mean $\langle T_1/T_2 \rangle$ ratio. In the sandstone plots (d–f) the vertical dashed lines indicate the mean $\langle T_1 \rangle$ for all values of T_2. The contour intervals are the same in all of these plots. The projections onto the T_1 and T_2 axes are shown in each case; the vertical scale on these projections are dimensionless functions $P\log(T_1/s)$ and $P\log(T_2/s)$, respectively.

at short relaxation times representing brine solution in small pores and the peaks at long relaxation times representing brine solution in large pores. However, in other work X-ray CT studies of similar rock types have revealed broad yet continuous pore size distributions [23] suggesting that this is not the origin of the two peaks. It is noted that additional peaks (artefacts) can be present in these two-dimensional correlations due either to the inversion procedure [24] or possibly as a result of the fluid flowing through magnetic susceptibilty induced field gradients. For these reasons, only the dominant peak was considered when determining the average $\langle T_1/T_2 \rangle$ ratio.

For the carbonate rock, Fig. 3(a–c), the dominant region can be seen to lie parallel to the line $T_1 = T_2$, providing a unique value of T_1 for each value of T_2. The value of $\langle T_1/T_2 \rangle$ was observed to increase with increasing flow rate from $\langle T_1/T_2 \rangle = 3.0$ at $Q = 1$ ml min^{-1}, Fig. 3(a, dashed diagonal line), to $\langle T_1/T_2 \rangle = 4.5$ at $Q = 16$ ml min^{-1}, Fig. 3(c, dashed diagonal line). This variation was due almost entirely to the change in $\langle T_2 \rangle$ of the flowing spins observed in Fig. 2(a–c). In the case of the sandstone, Fig. 3(d–f), the dominant peak is not orientated so as to lie parallel to the line $T_1 = T_2$. Instead only a single T_1 component appears to exist for all values of T_2 at each superficial flow velocity. The mean values of $\langle T_1 \rangle$, see Fig. 3(d–f, dashed vertical lines), were therefore used to remove the T_1 relaxation weighting from the corresponding propagator probability distributions.

The flow propagator probability distributions $P^*(\zeta^*, \Delta)$, determined without relaxation weighting from the combination of $\zeta - T_2$ and $T_1 - T_2$ correlations, see Figs. 2 and 3, respectively, are shown in Fig. 4(solid lines) for (a–c) carbonate and (d–f) sandstone rock cores with superficial flow velocities of (a,d) $Q = 1$ ml min^{-1}, (b,e) 5 ml min^{-1}, and (c,f) 16 ml min^{-1} and an observation time $\Delta = 1$ s. The equivalent uncorrected probability distributions $P(\zeta, \Delta)$, Fig. 4(dashed lines), are shown for comparison. Although not obvious from these plots, the removal of the relaxation time weighting has altered the spectral weight of the distributions. This is more pronounced in the case of the carbonate, Fig. 4(a–c), where a larger range of T_1 and T_2 relaxation times were present in the spin populations.

The true mean displacements $\langle \zeta \rangle^*$ extracted from the probability distributions without relaxation weighting are shown in Fig. 5(a) and (b) for the carbonate and sandstone rock cores, respectively.

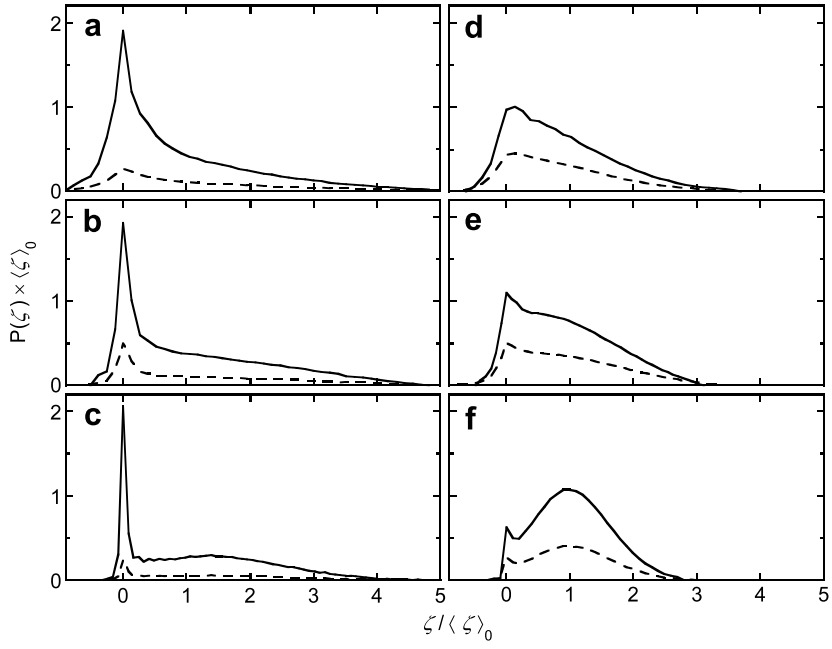

Fig. 4. Propagator probability distributions for brine flowing through (a–c) carbonate and (d–f) sandstone rock cores with imposed flow velocities of (a and d) $Q = 1$, (b and e) 5, and (c and f) 16 ml min^{-1}, at an observation time of $\Delta = 1$ s. The data shown are: $P(\zeta, \Delta)$ (dashed lines), $P^*(\zeta^*, \Delta)$ (solid lines). In all cases the probability density P and the displacement ζ have been normalised to dimensionless parameters using the expected mean displacement $\langle \zeta \rangle_0$.

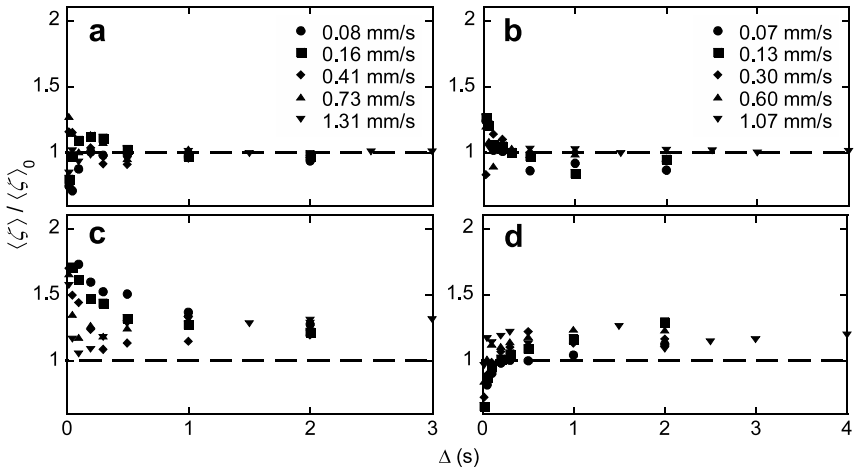

Fig. 5. Variation of the displacement with respect to the expected mean displacement $\theta = \langle\zeta\rangle/\langle\zeta\rangle_0$ as a function of observation time Δ for brine flowing through (a and c) carbonate and (b and d) sandstone rock cores. The upper graphs (a and b) show the relaxation corrected displacements $\langle\zeta\rangle^*$ where, at large displacements, $\theta^* \to 1$ for both samples. The lower graphs (c and d) show the uncorrected displacements $\langle\zeta\rangle$, where $\theta \to 1.29$ for the carbonate (c) and $\theta \to 1.18$ for the sandstone (d). In all cases the dashed horizontal lines represent $\theta = 1$.

It can be seen that, for long observation times and/or high flow rates corresponding to displacements of $\langle\zeta\rangle_0 \geqslant 300$ μm, $\theta^* \to 1$ for both rock samples. This is in contrast to the uncorrected mean displacements $\langle\zeta\rangle$ shown in Fig. 5(c) and (d) for the carbonate and sandstone rock cores, respectively. Here, $\theta \to 1.29$ for the carbonate, and $\theta \to 1.18$ for the sandstone. There is still a distortion in the θ^* data at short displacements where $\langle\zeta\rangle_0 < 300$ μm. This is due to insufficient q-space sampling—as a result of the maximum gradient being limited to $g_z^{max} = 10.7$ G cm^{-1}—which leads to Fourier artefacts in the probability distribution.

Additional complications can occur in the analysis if the T_1/T_2 ratio is a complex function of displacement. In the $T_1 - T_2$ correlation experiment, the T_1 recovery delays span times from $T = 10$ ms to 10 s. The determined relaxation time correlation will therefore contain components sensitive to motions averaged over a range of displacements. Since the T_1/T_2 ratio used in the correction process is determined from the dominant region in the $T_1 - T_2$ correlation plots, this could lead to an error in the corrected propagator probability distributions at short observation times and hence displacements. In the examples presented here this situation is not apparent: for the carbonate rock T_1/T_2 is constant over all values of T_2, and for the sandstone rock T_1 is invariant; see Fig. 3.

Furthermore, in some systems diffusive exchange can occur between spin populations. Cross-peaks in the $T_1 - T_2$ correlations are indicative of exchange between different regions of porosity [25,26], although no such peaks are observed in the rocks studied here. Exchange between stagnant and flowing spin populations can be observed as a variation in the intensity of the stagnant peak in the propagator probability distribution as a function of Δ [27]. This has been studied and simulated previously [28] and discussed for flow in permeable rocks [2]. Such exchange mechanisms could lead to the observed relaxation times being averaged on a different time-scale to the observed displacements. These complications will be considered in further detail in future work, where it may also be necessary to consider the effective "shutter speed" of the experiment defined by the values of q and the exchange rate [29]. At high flow velocities or long observation times, the range of q required to observe the displacement is reduced, so this affect will be less significant.

4.2. Flow propagator moments

The higher order moments of the flow propagators are also affected by the removal of the relaxation weighting. The second moment, or rms width, can be seen in Fig. 6(a) and (b) for the carbonate and sandstone rock cores, respectively. The uncorrected moments σ are represented by open circles (○), the "delta-function" corrected moments σ' are represented by open squares (□), and the true moments without relaxation weighting σ^* are represented by filled triangles (▲). σ and σ' were obtained using the APGSTE pulse sequence, Fig. 1(a), and are in good agreement with other data published for the same types of rock [2,16]. It is immediately obvious that the normalised σ^* lies between the two extremes of σ and σ' for both rocks as expected. The power-law fits to these data are summarised in Table 2. For both rocks the exponent η' is slightly larger than the equivalent true value of η^*, again as expected. It is reasonable to assume, from these results, that the second moments derived from the "delta-function" correction provide a value of η' between 5% and 10% larger than the true value η^*. The displacements l are seen to agree qualitatively with the degree of heterogeneity in the rock pore structures: larger dispersivities are observed in the comparatively heterogeneous carbonate compared to the more homogeneous sandstone [2].

The third moment, represented here as the normalised redefined skewness [2], should decrease asymptotically to zero with increasing displacement as the probability distribution tends to a Gaussian. In Fig. 6(c) and (d), for carbonate and sandstone, respectively, the different symbols represent the uncorrected third moments γ (○), the "delta-function" corrected third moments γ' (□), and the true third moments without relaxation weighting γ^* (▲). The three different data sets in each plot are seen to be similar; the only noticeable deviation occurs for $\langle\zeta\rangle \geqslant 1000$ μm. Here the normalised γ and γ' appear to reach a plateau—this is certainly expected of γ' due to the inclusion of the delta function at zero displacement—whereas γ^* continues to decrease toward zero. This deviation between the data sets is more pronounced in the sandstone core, Fig. 6(d). For both rocks the behaviour of γ^* above $\langle\zeta\rangle = 1000$ μm suggests the true propagator shape is more Gaussian than indicated by the uncorrected and "delta-function" corrected data.

5. Conclusion

In this paper we have detailed a methodology for determining NMR flow propagators without the influence of spin relaxation. This requires a combination of $\zeta - T_2$ [6] and $T_1 - T_2$ [21] two-dimensional correlations to quantify the signal loss due to both longitudinal and transverse relaxation throughout the entire APG-

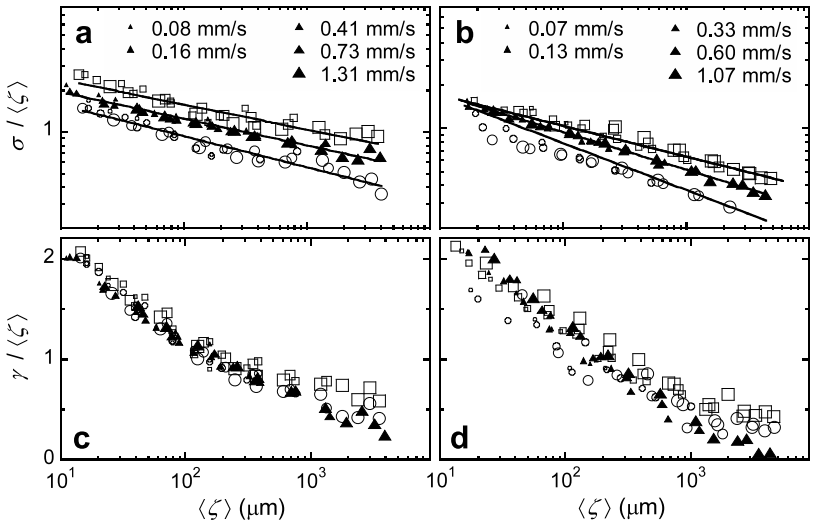

Fig. 6. Normalised (a and b) second and (c and d) third moments of the propagators for brine solution flowing through (a and c) carbonate and (b and d) sandstone rock cores. In each graph the symbols represent uncorrected moments σ and γ (○), "delta-function" corrected moments σ' and γ' (□), and moments without relaxation weighting σ^* and γ^* (▲). The size of the symbols indicates the mean pore velocity as given by the legends (shown for the ▲ symbols only). In (a) and (b) the solid lines indicate the power-law fits with the parameters given in Table 2. The observation times ranged from Δ = 100 ms to 4 s.

Table 2
Parameters for the power-law fit to $\sigma/\langle\zeta\rangle = (\langle\zeta\rangle/l)^{\eta}$ for the data shown in Fig. 6(a) and (b) for the carbonate and sandstone rock cores, respectively

Rock	l/μm	η	l^*/μm	η^*	l'/μm	η'
Carbonate	434	−0.23	758	−0.19	1054	−0.18
Sandstone	169	−0.36	199	−0.25	209	−0.22

These are determined from the uncorrected second moment σ, the second moments without relaxation weighting σ^*, and the "delta-function" corrected second moments σ'.

STE pulse sequence. In order to remove the T_1 weighting from the propagators, it is necessary to assume the T_1/T_2 ratio is not a function of observation time Δ. Furthermore, the $T_1 - T_2$ correlations, obtained under flow, must exhibit a unique T_1 component for each corresponding T_2 component. This method is suitable for acquiring flow propagator measurements where the mean advective displacement is greater than the mean diffusive displacement and where sufficient gradient strengths are available to explore the range of q-space necessary to avoid truncation errors in the Fourier transform. We have demonstrated the feasibility of these measurements within this regime by showing the true mean displacement, without relaxation time weighting, is equal to the expected mean displacement for brine solution flowing through carbonate and sandstone rock cores.

These measurements also provide an indication of the expected deviation in the dispersivity estimated from a "delta-function" correction [2], based on an upper limit assumption, compared to the true dispersivity. The "delta-function" correction is seen to overestimate the higher order moments as expected, and hence the dispersivity. In future publications we shall discuss the possibility of using rapid techniques to improve the efficiency of data acquisition in the two-dimensional correlations, offering the potential to determine the moments of the propagators without relaxation weighting in time sensitive measurements.

Acknowledgments

We thank Dr. Uli Scheven, REQUIMTE/CQFE, Portugal, for use of the propagator analysis protocol; Dr. Silke Sheppard, Schlumberger Cambridge Research, for providing the samples; and Dr. Andy Sederman for assistance with the experiments. We thank Mr. Michael Li, University of New Brunswick, Canada, and Mr. Mark Sankey for providing the phase cycle given in Table 1. J.M. thanks Mr Thusara Chandrasekera and Mr. Jonathan Griffith for use of their 1D Laplace Transform algorithm. For financial support J.M. thanks Schlumberger Cambridge Research. Thanks go to EPSRC for funding D.A.G. on Grant EP/C548817/1, and D.J.H. on Grant EP/C547195/1. Additional funding was supplied from Platform Grant GR/S20789/01.

References

[1] J. Karger, W. Heink, The propagator representation of molecular-transport in microporous crystallites, J. Magn. Reson. 51 (1) (1983) 1–7.
[2] U.M. Scheven, D. Verganelakis, R. Harris, M.L. Johns, L.F. Gladden, Quantitative nuclear magnetic resonance measurements of preasymptotic dispersion in flow through porous media, Phys. Fluids 17 (11) (2005) 117107.
[3] U.M. Scheven, J.G. Seland, D.G. Cory, NMR-propagator measurements in porous media in the presence of surface relaxation and internal fields, Magn. Reson. Imaging 23 (2) (2005) 363–365.
[4] P.M. Singer, G. Leu, E.J. Fordham, P.N. Sen, Low magnetic fields for flow propagators in permeable rocks, J. Magn. Reson. 183 (2) (2006) 167–177.
[5] U.M. Scheven, Stray field measurements of flow displacement distributions without pulsed field gradients, J. Magn. Reson. 174 (2) (2005) 338–342.
[6] M.M. Britton, R.G. Graham, K.J. Packer, Relationships between flow and NMR relaxation of fluids in porous solids, Magn. Reson. Imaging 19 (3-4) (2001) 325–331.
[7] M.M. Britton, R.G. Graham, K.J. Packer, NMR relaxation and pulsed field gradient study of alginate bead porous media, J. Magn. Reson. 169 (2) (2004) 203–214.
[8] C.W. Windt, F.J. Vergeldt, H. Van As, Correlated displacement-T_2 MRI by means of a Pulsed Field Gradient-Multi Spin Echo method, J. Magn. Reson. 185 (2) (2007) 230–239.
[9] E.O. Stejskal, J.E. Tanner, Spin diffusion measurements: spin echoes in the presence of a time-dependent field gradient, J. Chem. Phys. 42 (1) (1965) 288–292.
[10] E.L. Hahn, Spin echoes, Phys. Rev. 80 (4) (1956) 580–594.
[11] R.M. Cotts, M.J.R. Hoch, T. Sun, J.T. Markert, Pulsed field gradient stimulated echo methods for improved NMR diffusion measurements in heterogeneous systems, J. Magn. Reson. 83 (2) (1989) 252–266.
[12] P.G. de Gennes, Hydrodynamic dispersion in unsaturated porous-media, J. Fluid Mech. 136 (1983) 189–200.
[13] R. Kubo, M. Toda, N. Hashitsume, Statistical physics II: nonequilibrium statistical mechanics, Springer, Berlin/London, 1991.
[14] P.P. Mitra, P.N. Sen, L.M. Schwartz, P. Ledoussal, Diffusion propagator as a probe of the structure of porous-media, Phys. Rev. Lett. 68 (24) (1992) 3555–3558.
[15] J.P. Stamps, B. Ottink, J.M. Visser, J.P.M. van Duynhoven, R. Hulst, Difftrain: a novel approach to a true spectroscopic single-scan diffusion measurement, J. Magn. Reson. 151 (1) (2001) 28–31.

[16] J. Mitchell, A. Sederman, E.J. Fordham, M.L. Johns, L.F. Gladden, A rapid measurement of flow propagators in porous rocks, J. Magn. Reson. doi:10.1016/j.jmr.2007.12.014.
[17] M.D. Hurlimann, Effective gradients in porous media due to susceptibility differences, J. Magn. Reson. 131 (2) (1998) 232–240.
[18] M.H.G. Amin, S.J. Gibbs, R.J. Chorley, K.S. Richards, T.A. Carpenter, L.D. Hall, Study of flow and hydrodynamic dispersion in a porous medium using pulsed-field-gradient magnetic resonance, Proc. R. Soc. Lond. A Mat. 453 (1958) (1997) 489–513.
[19] E.J. Fordham, S.J. Gibbs, L.D. Hall, Partially restricted diffusion in a permeable sandstone—observations by stimulated echo PFG NMR, Magn. Reson. Imaging 12 (2) (1994) 279–284.
[20] S. Meiboom, D. Gill, Modified spin-echo method for measuring nuclear relaxation times, Rev. Sci. Instrum. 29 (1985) 668–691.
[21] Y.Q. Song, L. Venkataramanan, M.D. Hurlimann, M. Flaum, P. Frulla, C. Straley, T-1-T-2 correlation spectra obtained using a fast two-dimensional laplace inversion, J. Magn. Reson. 154 (2) (2002) 261–268.
[22] L. Venkataramanan, Y.Q. Song, M.D. Hurlimann, Solving Fredholm integrals of the first kind with tensor product structure in 2 and 2.5 dimensions, IEEE Trans. Signal Process 50 (5) (2002) 1017–1026.
[23] C.H. Arns, A comparison of pore size distributions derived by NMR and X-ray-CT techniques, Physica A 339 (1–2) (2004) 159–165.
[24] K.E. Washburn, P.T. Callaghan, Tracking pore to pore exchange using relaxation exchange spectroscopy, Phys. Rev. Lett. 97 (17) (2006) 175502.
[25] P.J. McDonald, J.P. Korb, J. Mitchell, L. Monteilhet, Surface relaxation and chemical exchange in hydrating cement pastes: a two-dimensional NMR relaxation study, Phys. Rev. E 72 (1) (2005) 011409.
[26] N. Marigheto, L. Venturi, D. Hibberd, K.M. Wright, G. Ferrante, B.P. Hills, Methods for peak assignment in low-resolution multidimensional NMR cross-correlation relaxometry, J. Magn. Reson. 187 (2) (2007) 327–342.
[27] U. Tallarek, T.W.J. Scheenen, H. Van As, Macroscopic heterogeneities in electroosmotic and pressure-driven flow through fixed beds and low column-to-particle diameter ratio, J. Phys. Chem. B 105 (36) (2001) 8591–8599.
[28] U.M. Scheven, J.G. Seland, D.G. Cory, NMR propagator measurements on flow through a random pack of porous glass beads and how they are affected by dispersion, relaxation, and internal field inhomogeneities, Phys. Rev. E 69 (2) (2004) 021201.
[29] J.H. Lee, C.S. Springer, Effects of equilibrium exchange on diffusion-weighted NMR signals: the diffusigraphic "shutter-speed", Magn. Reson. Med. 49 (1) (2003) 450–458.